Journal of Applied Physics

Impurity-hydrogen complexes in β-Ga_2O_3: Hydrogenation of shallow donors vs deep acceptors

Cite as: J. Appl. Phys. **131**, 035706 (2022); https://doi.org/10.1063/5.0080341
Submitted: 30 November 2021 • Accepted: 29 December 2021 • Published Online: 20 January 2022

Andrew Venzie, Amanda Portoff, E. Celeste Perez Valenzuela, et al.

Journal of Applied Physics ARTICLE scitation.org/journal/jap

Impurity-hydrogen complexes in β-Ga_2O_3: Hydrogenation of shallow donors vs deep acceptors

Cite as: J. Appl. Phys. **131**, 035706 (2022); doi: 10.1063/5.0080341
Submitted: 30 November 2021 · Accepted: 29 December 2021 ·
Published Online: 20 January 2022

Andrew Venzie,[1] Amanda Portoff,[1] E. Celeste Perez Valenzuela,[1] Michael Stavola,[1,a)] W. Beall Fowler,[1] Stephen J. Pearton,[2] and Evan R. Glaser[3]

AFFILIATIONS

[1]Department of Physics, Lehigh University, Bethlehem, Pennsylvania 18015, USA
[2]Department of Materials Science and Engineering, University of Florida, Gainesville, Florida 32611, USA
[3]U.S. Naval Research Laboratory, Electronics Science and Technology Division, Code 6882, Washington, DC 20375, USA

Note: This paper is part of the Special Topic on Defects in Semiconductors.
[a)]**Author to whom correspondence should be addressed:** michael.stavola@Lehigh.edu

ABSTRACT

Substitutional impurities in β-Ga_2O_3 are used to make the material n-type or semi-insulating. Several O–H and O–D vibrational lines for complexes that involve impurities that are shallow donors and deep acceptors have been reported recently. The present article compares and contrasts the vibrational properties of complexes that involve shallow donors (OD-Si and OD-Ge) with complexes that involve deep acceptors (OD-Fe and OD-Mg). Theoretical analysis suggests that these results arise from defect complexes based on a shifted configuration of the Ga(1) vacancy with a trapped H atom and a nearby impurity.

I. INTRODUCTION

β-Ga_2O_3 is a transparent conducting oxide with an ultra-wide bandgap (~4.8 eV) that attracts much recent attention for high-power, deep-UV, and extreme environment applications.[1–7] β-Ga_2O_3 has a monoclinic structure with two inequivalent Ga sites [fourfold coordinated Ga(1) and sixfold coordinated Ga(2)] and three inequivalent oxygen sites.[8,9] Defects and impurities strongly affect the conductivity of Ga_2O_3.[10] Undoped bulk Ga_2O_3 is typically n-type with a free-carrier concentration near 10^{17} cm^{-3}.[4,7,10,11] Fe impurities that introduce a deep acceptor state that compensates the n-type doping are also prevalent in bulk Ga_2O_3.[7,12] Hydrogen is also frequently present in oxide semiconductors where it introduces shallow donors and passivates deep acceptors.[13–15] The situation for Ga_2O_3 has been found to be similar where hydrogen gives rise to shallow donors[16,17] and where a deep acceptor like the Ga vacancy (V_{Ga}) has been found to form stable complexes with H.[18] Vibrational spectroscopy performed with polarized light has proven to be a powerful probe of hydrogen centers in Ga_2O_3.[19–21]

Substitutional impurities help to determine the conductivity of Ga_2O_3. Si and Ge impurities at a Ga(1) site and Sn at a Ga(2) site are shallow n-type dopants.[22,23] Si impurities are also responsible for unintentional n-type doping of Ga_2O_3.[24,25] Several other impurities act as deep acceptors in Ga_2O_3. Fe,[12,26] Mg,[28–30] and Zn[31,32] on a Ga(2) site in Ga_2O_3 give rise to deep acceptors that can make Ga_2O_3 semi-insulating. Fe-doped Ga_2O_3 substrates are commercially available.[33]

Both shallow dopants such as Si[34] and deep acceptors such as Fe,[34] Mg,[29] Ca,[35,36] and Zn[31] interact with hydrogen to form OH-impurity complexes. In the present article, we compare and contrast the vibrational properties of OD-impurity complexes that contain shallow donors with those that contain deep acceptors. (We favor the study of the ^{2}H deuterium isotope in our experiments rather than ^{1}H because the vibrational lines for D can be detected with a greater signal-to-noise ratio.) The implications of these results for the defect structures of OD-impurity complexes that are likely to be formed are discussed.

II. EXPERIMENTAL METHODS

Ga_2O_3 samples containing shallow donors and deep acceptors have been investigated in our experiments. Undoped and intentionally Fe-doped, bulk Ga_2O_3 samples with both (010) and $(\bar{2}01)$ faces were purchased from the Tamura Corporation (Novel Crystal Technology). Mg-doped Ga_2O_3 samples for our studies were grown by the Czochralski method at Synoptics.

Si-doped epitaxial layers of Ga_2O_3 that had been grown by molecular beam epitaxy (MBE) were purchased from Novel Crystal Technology. These epi-layers were 0.5 μm thick and doped with Si to a nominal concentration of 2×10^{18} cm^{-3}. The (010) semi-insulating Ga_2O_3 substrate for the MBE growth was doped with Fe. Ge-doped layers of Ga_2O_3 were prepared by ion implantation with multiple energies and doses and annealed in O_2 for 120 s at 1100 °C under the conditions given previously[37] to produce Ge-doped layers approximately 1 μm thick with concentration [Ge] = 1×10^{19} cm^{-3}.

Ga_2O_3 samples with thin doped layers were treated in H- or D-plasmas for 30 min at a nominal temperature of 150 °C to introduce hydrogen and/or deuterium. Bulk samples were hydrogenated by annealing at 900–1000 °C for several hours in sealed quartz ampoules that contained H_2 or D_2 gas (~2/3 atm at room temperature). The slight degradation of the sample surfaces by these treatments did not affect the study of bulk defects by infrared (IR) spectroscopy.

Infrared (IR) absorption spectra were measured with a Nicolet iS50 Fourier transform IR spectrometer equipped with a CaF_2 beamsplitter and a liquid N_2-cooled InSb detector. The polarization of the transmitted light was analyzed with a wire-grid polarizer placed after the sample. Samples were cooled for our measurements with liquid He or liquid N_2 in a Helitran continuous flow cryostat.

β-Ga_2O_3 has a low-symmetry monoclinic structure that makes the vibrational absorption anisotropic. Polarized absorption measurements have been made for Ga_2O_3 samples with either a $(\bar{2}01)$ face or a (010) face to obtain information about the orientations of the transition moments of the different O–D centers that are of interest. β-Ga_2O_3 has principal dielectric axes, X, Y, Z (Ref. 38). The Y axis is taken to be along the [010] optic axis of the crystal. The frequency-dependent orientations of the perpendicular X and Z axes were determined previously by ellipsometry over a broad spectral range[37] and were also determined from the polarization dependence of the vibrational absorption in the IR spectral range that is of interest here.[21]

Annealing treatments were performed in a tube furnace in a flowing Ar ambient. Secondary ion mass spectrometry (SIMS) measurements were performed by the Evans Analytical Group. The detection limits for Fe and Mg impurities were quoted to be 1×10^{15} and 1×10^{14} cm^{-3}, respectively.[39]

III. EXPERIMENTAL RESULTS

Figure 1 shows IR absorption spectra (5 K, resolution 0.25 cm^{-1}) for a Si-doped epitaxial layer with [Si] = 2×10^{18} cm^{-1} that was grown by MBE on a (010) Fe-doped substrate. (This is the same sample whose spectra measured at 77 K were reported previously.)[34] This sample was treated in a plasma that contained both H and D to simultaneously introduce both hydrogen isotopes into the sample. The O–D lines at 2579.1 and 2586.0 cm^{-1} were

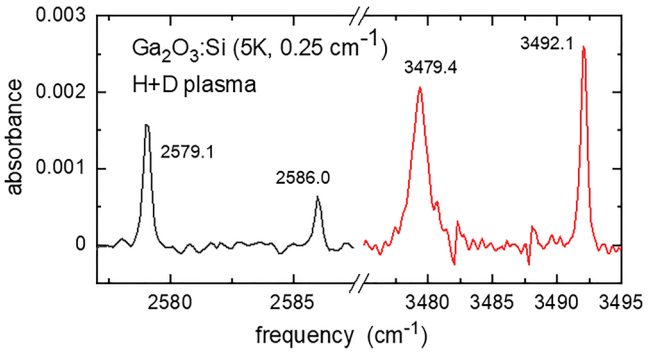

FIG. 1. IR spectrum (5 K, resolution 0.25 cm^{-1}) of a Si-doped Ga_2O_3 epitaxial layer grown on an Fe-doped substrate treated in a plasma containing both H and D. IR lines arising from H (shown in red) and D (shown in black) in both the thin epitaxial layer and the Fe-doped substrate are observed.

assigned to OD-Si and OD-Fe complexes in Ga_2O_3, respectively.[34] Lines at 3479.4 and 3492.1 cm^{-1} were assigned to the corresponding OH-Si and OH-Fe complexes.[34] (The frequency ratio, $r = \omega_H/\omega_D = 1.349$, for these lines is consistent with H bonded to a light atom like O).[19]

The presence of sharp IR lines without any additional sidebands or a structure for samples that contain both H and D is a signature of defects that contain a single H or D atom.[19] The spectrum shown in Fig. 1 strengthens the conclusions of Ref. 34 by showing that spectra measured at lower T and higher resolution reveal only sharp vibrational lines without any of the additional structure that would be characteristic of a multi-H center that could contain both hydrogen isotopes. These results confirm that the OD-Si and OD-Fe complexes assigned in Ref. 34, whose spectra are shown in Fig. 1, contain a single D atom.

The spectrum in Fig. 1 shows OH-impurity complexes for which the impurities are a shallow donor (Si) and a deep acceptor (Fe). The O–H (O–D) lines have similar frequencies in spite of the fact that the impurities lie on different Ga sites in the Ga_2O_3 lattice and have different electrical properties. We examine the properties of these defects in greater detail along with OH-impurity complexes with additional donor and acceptor impurities to investigate the differences in their microscopic properties.

A. Impurity dependence of the OH-impurity spectra

1. Shallow donor impurities

The vibrational spectra of OD-donor complexes are compared for Si and Ge donors in Fig. 2(a). The corresponding spectra for the OH-donor complexes are shown in Fig. 2(b). The upper spectrum in each panel shows the O–D (O–H) vibrational lines seen for Si-doped Ga_2O_3 grown by MBE, and the lower spectrum shows the O–D (O–H) lines seen for a sample doped with Ge by ion implantation. The frequency ratio for the OH-Ge and OD-Ge lines at 3425.0 and 2539.8 cm^{-1}, respectively, is $r = \omega_H/\omega_D = 1.349$, similar to the value of r for Si-containing complexes.

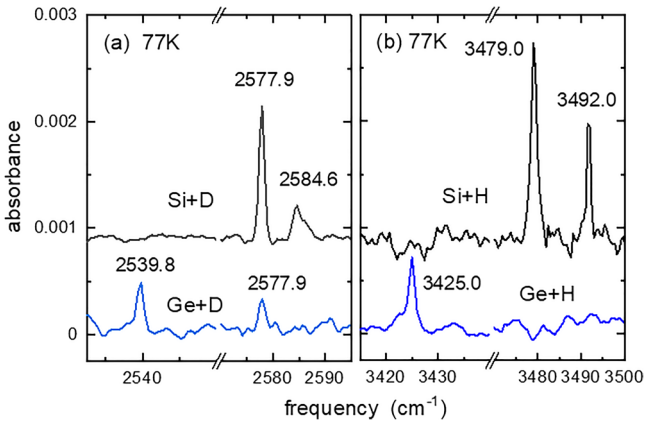

FIG. 2. IR spectra (77 K, resolution 1 cm^{-1}) that compare a Si-doped Ga_2O_3 epitaxial layer (upper spectra, shown in black) with a Ge-doped layer produced by ion implantation (lower spectra, shown in blue). The samples in (a) were treated in a D plasma and the samples in (b) were treated in a H plasma (30 min, 150 °C).

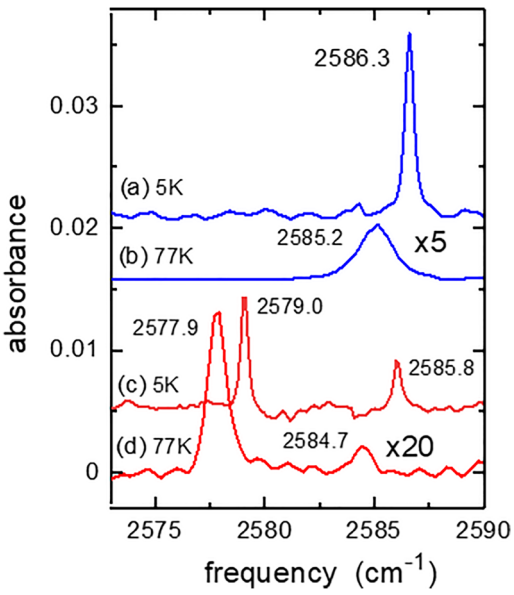

FIG. 3. IR absorbance spectra measured at 5 K with a resolution of 0.25 cm^{-1} [(a) and (c)] and at 77 K with a resolution of 1 cm^{-1} [(b) and (d)] for (010) Ga_2O_3 samples. The lines in spectra (a) and (b) (shown in blue) have been assigned to the OD-Mg complex. The lines in spectra (c) and (d) (shown in red) have been assigned to the OD-Si and OD-Fe complexes. Spectra (a) and (b) were measured for a bulk, Ga_2O_3 sample doped with Mg and deuterated by annealing in a D_2 ambient (5 h, 1000 °C). Spectra (c) and (d) were measured for a Si-doped epitaxial layer grown on an Fe-doped substrate that was deuterated by a treatment in a D plasma. (The IR measurements probe O–D centers in both the epilayer and substrate.)

The vibrational frequency of the OD-Ge complex is 35.1 cm^{-1} lower than that of the OD-Si complex. Similarly, the O–H frequency for the OH-Ge complex lies 54.0 cm^{-1} lower than that of the corresponding Si-containing defect. These sizable frequency shifts suggest a defect structure with the O–D (or O–H) group in close proximity to the donor impurity or, alternatively, two different defect structures.

2. Deep acceptor impurities

Fe in Ga_2O_3 has been found by electron paramagnetic resonance (EPR) to preferentially occupy the octahedral Ga(2) site in Ga_2O_3[26] in agreement with theory that finds that Fe at the Ga(2) site has a lower formation energy than Fe at a tetrahedral Ga(1) site.[12] The electrical levels introduced by Fe in Ga_2O_3 have been studied by deep-level-transient spectroscopy (DLTS)[12] and EPR.[26,27] The DLTS peak E2 has a level 0.78 eV below the conduction band edge and was found to track the Fe concentration determined independently by SIMS over a wide range of Fe concentrations.[12] EPR studies have also examined the position of the Fe acceptor level in Ga_2O_3.[26,27] The assignment of E2 to Fe at an octahedral site in Ga_2O_3 is strongly supported by EPR studies of the Fe^{2+}/Fe^{3+} transition.[26] Fe can be intentionally introduced into Ga_2O_3 at concentrations that exceed the unintentional donor concentration.[33]

Spectra for OD-impurity complexes are shown in Fig. 3 for samples that were intentionally doped with Fe and Mg. The line at 2584.7 cm^{-1} (77 K) was previously assigned to an OD-Fe complex based on its strength in samples doped deliberately with Fe and also its presence in several additional Ga_2O_3 samples because Fe is known to be a common unintentional contaminant.[40] For example, a line at 2583.7 cm^{-1} (77 K) was reported for undoped Ga_2O_3 annealed in a D_2 ambient that is likely to arise from the OD-Fe complex.[41]

O–H (O–D) vibrational lines for complexes containing other deep acceptors such as Mg,[29] Zn,[31] and Ca[35] have been reported at frequencies (10 K) 3492 (2586), 3486.7 (2582.9), and 3441 (2557) cm^{-1}, respectively. These deep acceptors have been considered as possible alternatives to Fe to make Ga_2O_3 semi-insulating. We focus here on the OD-Mg complex and a comparison of its vibrational properties with those of the OD-Fe center. EPR and theory find that the Mg ion sits on a sixfold coordinated Ga(2) site in Ga_2O_3.[28,30]

Figure 3 shows that the frequencies (77 K) of the O–D lines seen for samples deliberately doped with Fe and Mg lie at 2584.7 and 2585.2 cm^{-1}, respectively. These O–D lines lie sufficiently close in frequency at 77 K that it is difficult to be certain that the OD-Fe complex is not the defect being seen in both cases due to the adventitious nature of the Fe impurity in Ga_2O_3.[12,40]

Spectra measured at 5 K and at higher resolution (0.25 cm^{-1}) are also shown in Fig. 3. The frequencies (5 K) of the OD-impurity lines seen for deliberate Fe- and Mg-doped samples lie at 2585.8 and 2586.3 cm^{-1} and differ by 0.5 cm^{-1}. While these lines are separated by more than their linewidths, their difference in frequency is not larger than the typical sample-to-sample variations that are observed for the OD-Fe line frequency.

3. Temperature dependence

In an attempt to further distinguish between the OD-impurity lines for samples doped with different impurities, the temperature

dependences of the lines were measured. Figure 4 shows the line frequencies vs temperature for the OD-Si, OD-Fe, and OD-Mg complexes. The temperature dependences of the line frequencies could be conveniently fit with an expression developed by Persson and Rydberg [Eq. (1)] for the anharmonic coupling of a local vibrational mode (i.e., the O–D mode of interest here) with an exchange mode that may be a local mode or phonon that is anharmonically coupled to the phonon bath,[42]

$$(\omega - \omega_0) = \delta\omega / \left[\exp\left(\frac{E_0}{kT}\right) - 1\right]. \quad (1)$$

Here, ω_0 is the frequency of the local vibrational mode at low temperature, $\delta\omega$ is an anharmonic coupling parameter, and E_0 is the energy of the exchange mode. The parameters for the fits shown in Fig. 4 are listed in Table I. The shifts in the line frequencies for the OD-Si and OD-Fe complexes are sufficiently different for these defects to be easily distinguished. However, while the frequency shifts of the lines seen for Fe- and Mg-doped samples differ significantly from those seen for the OD-Si complex, they differ only slightly from each other. Parameters describing the shifts of the lines in Fe- and Mg-doped samples (Table I) are the same, within error.

B. Evidence for distinct OH-deep-acceptor complexes: SIMS and annealing data

1. SIMS data

While our spectroscopic results for vibrational lines assigned to OD-Fe and OD-Mg complexes do not clearly indicate that two different defects are being seen, SIMS results (Fig. 5) show that the Fe and Mg concentrations are substantially different for our samples doped intentionally with these impurities. Figure 5(a) shows that the Mg concentration is more than two decades smaller than the Fe concentration in our deliberately Fe-doped sample. Figure 5(b) shows that the Fe concentration is more than a decade smaller than the Mg concentration in the deliberately Mg-doped sample. The SIMS results in Fig. 5 support the suggestion that different OD-Fe and OD-Mg complexes with very similar vibrational properties are formed in samples deliberately doped with Fe and Mg, respectively.

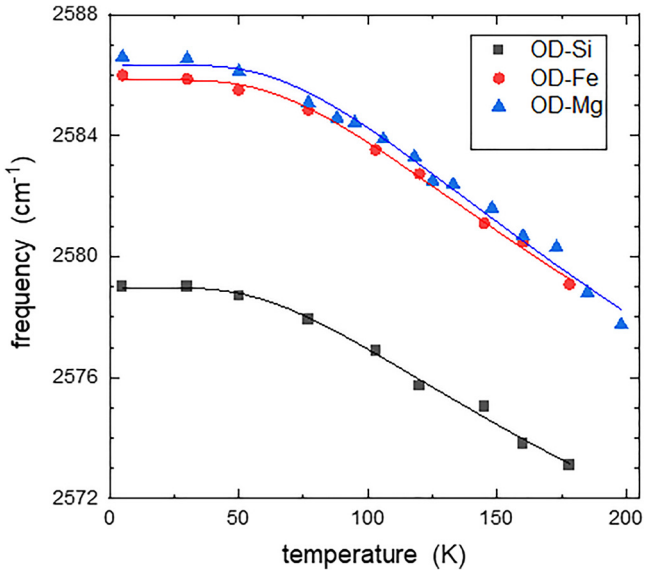

FIG. 4. Temperature dependences for the IR lines assigned to the OD-Si, OD-Fe, and OD-Mg complexes for the same samples whose data are shown in Fig. 3.

TABLE I. Frequencies (5 K) of the OD-impurity complexes in Ga_2O_3 and the parameters describing their shift with temperature [Eq. (1)].

Impurity	ω_0 (cm^{-1})	$\delta\omega$ (cm^{-1})	E_0 (cm^{-1})
Si	2579.0 ± 0.1	−22.0 ± 2.4	163 ± 13
Fe	2585.8 ± 0.1	−28.5 ± 2.6	180 ± 11
Mg	2586.3 ± 0.2	−31.6 ± 3.4	187 ± 14

2. Annealing results

In another attempt to distinguish between the O–D lines seen for Fe- and Mg-doped samples, we have examined the annealing stabilities of these lines. The absorbance of the O–D lines vs the temperatures of sequential annealing treatments (30 min) is plotted in Fig. 6. [The defects of interest here have different polarization properties. The OD-Fe and OD-Mg complexes have strongest absorption for **E**//Z, while the O–D line at 2547^{-1} assigned previously to the V_{Ga}-2D center[18] has strongest absorption for **E**//X. (The orientations of the X and Z dielectric axes are given in Sec. III C.)].

The annealing results for the Fe-doped sample are similar to those reported previously.[34] The 2485 cm^{-1} line seen for polarization **E**//Z assigned to the OD-Fe complex is annealed away near 350 °C. When the OD-Fe complex releases its D, the O–D line at 2547 cm^{-1} due to the V_{Ga}-2D complex[18] appears for polarization **E**//X. The 2547 cm^{-1} line is then annealed away at 450 °C.

For the Mg-doped sample, the O–D line at 2585 cm^{-1} is the dominant line seen in the sample and is thermally stable up to 650 °C. When the 2585 cm^{-1} line is annealed away, no other O–D lines appear, consistent with D leaving the sample.

The difference in annealing stabilities for the 2585 cm^{-1} lines seen in Fe-doped and Mg-doped samples provides strong evidence for the existence of distinct OD-Fe and OD-Mg complexes with very similar vibrational properties.

C. Polarization dependence of the O–D vibrational lines

The polarization dependence of the O–H (O–D) spectra reveals the orientation of the transition moment of a defect and provides structure-sensitive information.[21] Spectra are shown in Fig. 7 for the OD-Fe and OD-Si complexes with the probing light propagating along the [$\bar{2}$01] direction and with polarizations **E**//[102] and **E**//[010]. There is no absorption observed for the

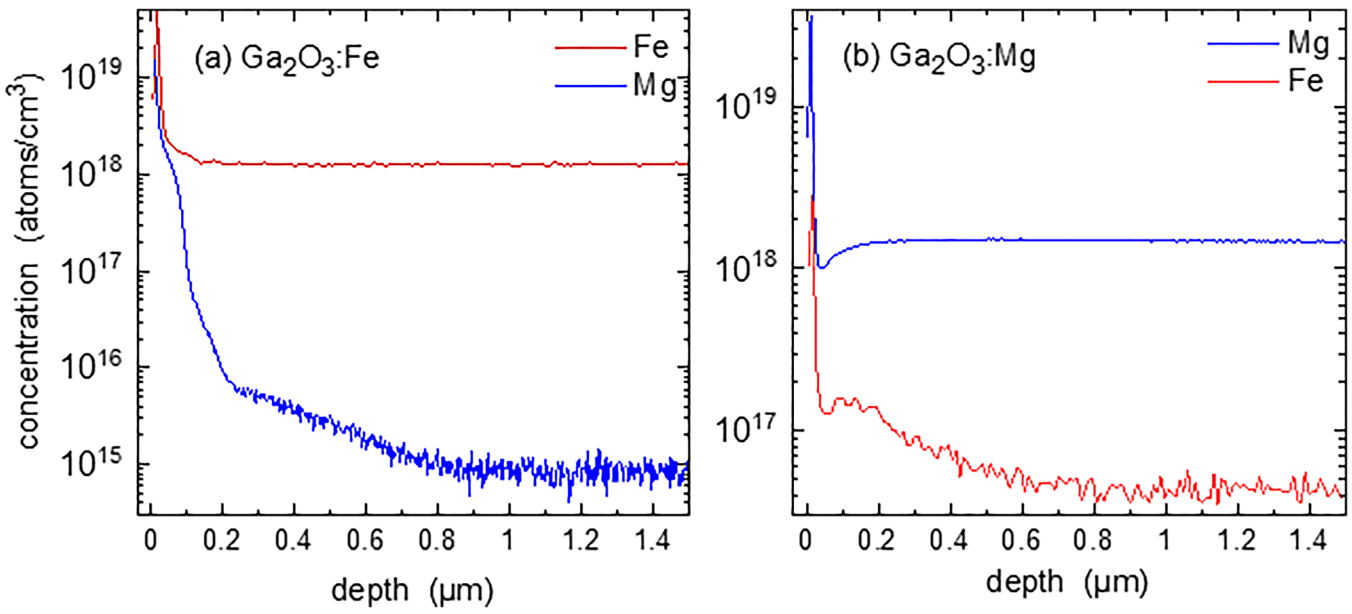

FIG. 5. SIMS profiles for Fe and Mg in Ga_2O_3 bulk samples intentionally doped (a) Fe and (b) Mg. The detection limits for Fe and Mg are 1×10^{15} and 1×10^{14} cm^{-3}, respectively.

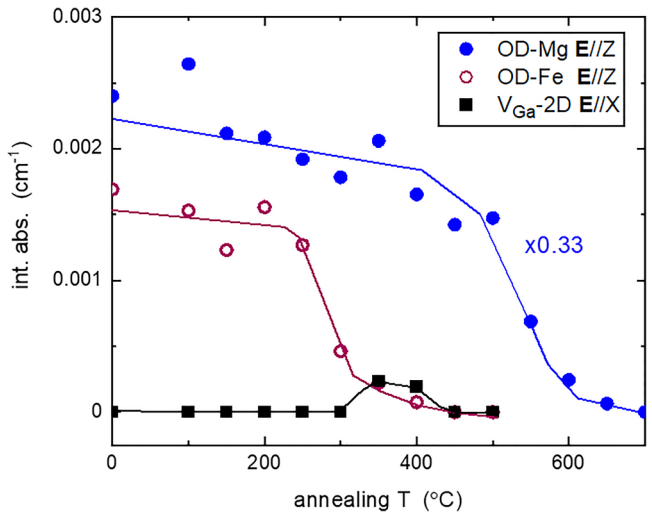

FIG. 6. Integrated absorbance for the IR lines assigned to the OD-Mg, OD-Fe, and V_{Ga}-2D complexes vs annealing temperature (30 min). The data shown are for the polarization directions that showed strongest absorption for the defect of interest. Results for OD-Mg were obtained from a (010) Mg-doped sample prepared by annealing in a D_2 ambient for 5 h at 1000 °C. Results for OD-Fe and V_{Ga}-2D were obtained from a separate (010) Fe-doped sample prepared by annealing in a D_2 ambient (6 h, 1000 °C).

OD-Si and OD-Fe complexes for **E**//[010] for two different samples, one intentionally doped with Fe [Fig. 7(a)] and the other unintentionally doped, presumably with Fe [Fig. 7(b)]. Results reported by others for the absorption lines assigned to the OH-Mg, OH-Zn, and OH-Ca complexes also show no absorption for

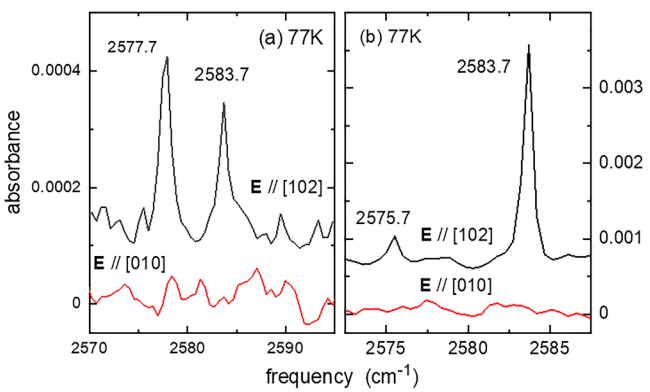

FIG. 7. Polarized IR absorbance spectra (77 K resolution, 1 cm^{-1}) for ($\bar{2}$01) Ga_2O_3 samples with the polarization directions shown. Samples were deuterated by annealing in a D_2 ambient (1000 °C, 5 h). The sample in (a) was deliberately doped with Fe and the sample in (b) was not intentionally doped.

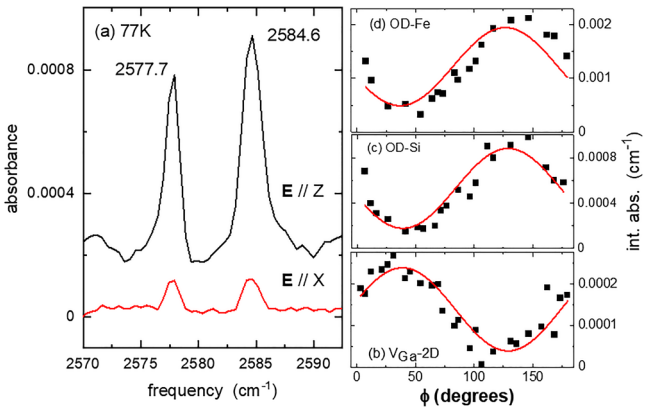

FIG. 8. (a) Polarized IR absorbance spectra (77 K resolution, 1 cm^{-1}) for a (010), Fe-doped Ga_2O_3 sample deuterated be an anneal at 1000 °C (6 h) in a D_2 ambient. Lines assigned to the OD-Si and OD-Fe complexes are shown for polarization directions that are indicated. Panels (b)–(d) show the integrated absorbance as a function of the angle of the transmission axis of an analyzing polarizer for IR lines assigned to the V_{Ga}-2D, OD-Si, and OD-Fe complexes, respectively. Data are fit with Eq. (2). The data for panel (c) were measured for the same sample whose spectrum is shown in panel (a). The data for panels (b) and (d) were measured for a (010) Fe-doped sample that had been treated in a D_2 ambient (1000 °C, 6 h). (d) was measured for the as-treated sample and (b) was measured following an additional anneal at 350 °C that produced the V_{Ga}-2D center.

E//(010).[29,31,35] The O–H and O–D centers that have been observed all have transition moments lying in the (010) plane.

Spectra are shown in Fig. 8(a) for light propagating along the [010] optic axis of β-Ga_2O_3 to investigate the directions of IR transition moments in the (010) plane. A strategy for analyzing the angular dependence of the absorption lines like those shown in Fig. 8(a) for the monoclinic structure of Ga_2O_3 is given in Ref. 21 and a monograph by Turrell.[43] Figure 9(a) shows the various axes and angles of interest here. The polarization of light polarized along a principal axis is maintained as it propagates through the crystal. The absorbance $A(\theta)$ is given by the log of the sum of the transmissions along the two principal axes X and Z [Eq. (2)],[21,43]

$$A(\theta) = -\log_{10}(\cos^2\theta\, e^{-\alpha_x l} + \sin^2\theta\, e^{-\alpha_z l}). \tag{2}$$

Here, l is the thickness of the sample and θ is the angle between the transmission axis of the analyzing polarizer and the X dielectric axis. The different O–H and O–D centers have absorption coefficients α_x and α_z for the X and Z principal axes [Eq. (3)][21,43] with

$$\alpha_x \propto \cos^2\chi/n_x \text{ and } \alpha_z \propto \sin^2\chi/n_z. \tag{3}$$

The refractive indices along the X and Z directions are given by $(n_z/n_x) = 1.892/1.865$ [see Eq. (2), Ref. 38].

Equation (2) shows that when the analyzing polarizer is along the X or Z axis (i.e., when θ is 0° or 90°), the extreme values of the

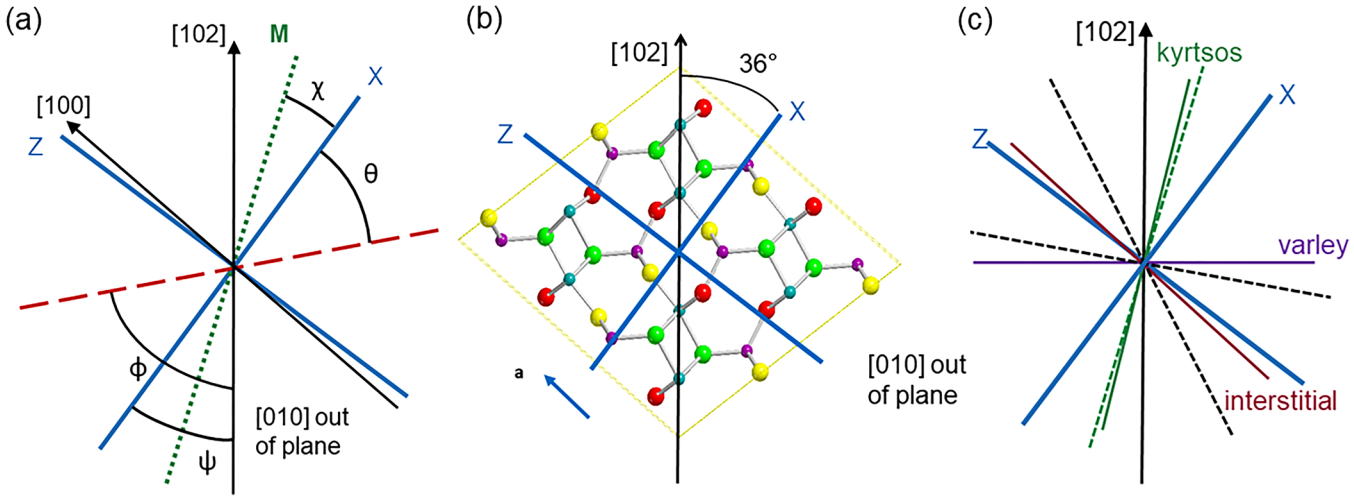

FIG. 9. (a) Definition of angles for optical absorption measurements of β-Ga_2O_3 with light incident along the (010) optic axis. The crystallographic (102) axis and the principal dielectric axes (X and Z) are shown. Three unique angles are referenced to the X axis: the first is χ, the orientation of the transition-dipole moment **M** of the defect; the second is ψ that gives the orientation of the (102) crystal axis; and θ is the angle for the transmission axis **E** of the polarization analyzer. The angle between **E** and the (102) axis that is varied experimentally is ϕ. (b) Orientations of the X and Z dielectric axes with respect to the crystal structure of β-Ga_2O_3. The inequivalent atomic sites are color coded as follows: Ga(1), purple; Ga(2), dark green; O(1), red; O(2), yellow; and O(3), light green. (c) Orientations of the transition moments for the different possible structures of the O–H centers that have been considered are shown by colored solid lines that are labeled by the configuration type. The orientations of the transition moments found by experiment for the V_{Ga}-2D (dashed green) and OD-impurity (dashed black) complexes are also shown.

angle-dependent absorbance are obtained, thus determining the angle ψ between the X and [102] axes. Since our previous study of the polarization dependence of the 2547 cm^{-1} line is assigned to the V_{Ga}-2D complex, we have studied the polarization dependences of four different O–D centers in five different oriented samples. These results have led us to revise our determination of the angle ψ of the X dielectric axis with respect to the [102] crystal axis in the IR range near 2500 cm^{-1}. Our collection of IR data yields an angle of $\psi = 36° \pm 4°$. (This result agrees with the result determined previously by ellipsometry,[38] within experimental error.) The orientations of the X and Z principal axes with respect to the Ga_2O_3 crystal structure are shown in Fig. 9(b).

The angle of the transition moment, χ, for an O–H or O–D center with respect to the X dielectric axis is determined from the dichroic ratio given in the following equation:[21,43]

$$D = \alpha_x/\alpha_z = (n_z/n_x)\cot^2\chi. \quad (4)$$

The dependences of the absorbances on the angle of the analyzing polarizer shown in Figs. 8(b)–8(d) were fit with Eq. (2) to determine the dichroic ratios and transition moment directions for the V_{Ga}-2D, OD-Si, and OD-Fe complexes that are given in Table II. Polarized absorption data were also measured for the 2585.1 cm^{-1} O–D line seen for the (010) β-Ga_2O_3 sample deliberately doped with Mg and deuterated by annealing in a D_2 ambient and are shown in Fig. 10. [The orientation of this Mg-doped sample in the (010) plane was determined optically from the 2620 cm^{-1} line that is also seen in Fig. 10(a) whose polarization dependence has been measured previously.][41,44] The dichroic ratio and the transition moment direction for the O–D line assigned to the OD-Mg complex shown in Fig. 10(a) were determined from a fit of Eq. (2) to the angle-dependent data shown in Fig. 10(b) and are also given in Table II. We emphasize the marked difference in the transition moment directions for the V_{Ga}-2D center and the OD-impurity complexes studied here. The angle of the transition moment for the V_{Ga}-2D center has been found to be $\pm$ 21° with respect to the X dielectric axis, whereas the angles of the transition moments for the OD- impurity complexes are greater than ±60°.

Results for the transition moment directions determined by experiment are shown in Fig. 9(c). The dashed green line shows the angle X = 21° counter-clockwise with respect to the X principal axis for the 2547 cm^{-1} line assigned to the V_{Ga}-2D complex.[18] (Our results do not determine the sign of the angle X so the opposite sign is also possible.) The dashed black lines show the angles ±64° for the 2577 cm^{-1} line assigned to the OD-Si complex.[34] (In this case, we show both signs of the angle X.) The transition moment directions for the OD-Fe and OD-Mg complexes lie within a few degrees of the results shown for the OD-Si complex.

TABLE II. The absolute value of the angle χ of the transition moment with respect to the X dielectric axis for O-D centers in Ga_2O_3. The angle $\psi \pm |\chi|$ gives the transition moment direction with respect to the [102] crystal axis.

Defect	V_{Ga}-2D	OD-Si	OD-Fe	OD-Mg
$\lvert\chi\rvert$	$21^\circ_{-12^\circ}+6^\circ$	$65° \pm 5°$	$64° \pm 5°$	$61° \pm 2°$
$\psi - \lvert\chi\rvert$	$15^\circ_{-11^\circ}+16^\circ$	$101° \pm 9°$	$100° \pm 9°$	$97° \pm 6°$
$\psi + \lvert\chi\rvert$	$57^\circ_{-16^\circ}+10^\circ$	$151° \pm 9°$	$152° \pm 9°$	$155° \pm 6°$

IV. ANALYSIS AND DEFECT MODELS

The collection of experimental data presented here combined with earlier work provide a framework that along with the results of theoretical calculations can yield plausible models for the structures of the OD-impurity complexes investigated here.

Three defect structures that bear leading consideration as candidates for the observations reported here are shown in Fig. 11. Figures 11(a) and 11(b) show two different shifted configurations of the Ga(1) vacancy, along with the associated H trapping sites. In the absence of trapped H, Fig. 11(b), which we call the Varley configuration,[16,45] is more stable than Fig. 11(a), the Kyrtsos configuration[46] (with the configurations named after the authors who proposed them). But with two trapped H, the Kyrtsos configuration is more stable[18,41] and leads to the primary observed 2547 cm^{-1} OD absorption line assigned to the V_{Ga}-2D complex. Figure 11(c) shows the site of an interstitial D trapped at an O(1). A second trapped interstitial D site between two O(2) is also possible but would yield IR absorptions lower than 1800 cm^{-1}, which would not be seen in our experiments and is not shown.

Each of these structures features a characteristic O–D direction with respect to (102): ∼15°–20° for Fig. 11(a), 90° for Fig. 11(b), and ∼120° for Fig. 11(c). The associated transition moment directions are also illustrated in Fig. 9(c) as solid lines labeled by the configuration type. Each, in turn, could serve as the basis for a perturbed structure with a neighboring Ga atom replaced by a metal impurity atom.

Polarization results, Figs. 8 and 10 and Table II, show clearly that while the Kyrtsos configuration [Fig. 11(a)] is consistent with the observed transition moment direction for V_{Ga}-2D, it cannot be considered for the defects perturbed by Fe, Si, or Mg. Thus, we turn to the Varley and trapped interstitial configurations as remaining candidates for those defects.

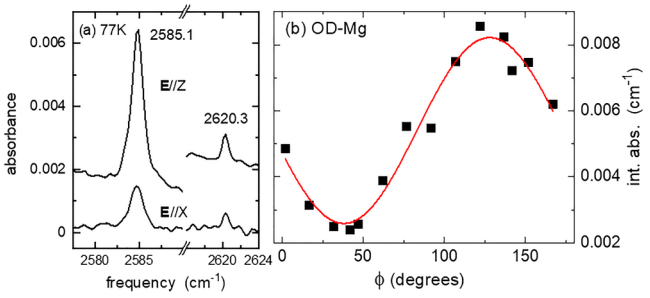

FIG. 10. (a) Polarized IR absorbance spectra (77 K resolution, 1 cm^{-1}) for a (010), Mg-doped Ga_2O_3 sample deuterated by annealing in a D_2 ambient (1000 °C, 5 h). Lines at 2585.1 and 2620.3 cm^{-1}—are shown for the polarization directions that are indicated. (The polarization of the line at 2620.3 cm^{-1} has been studied previously and was used to orient this sample.) (b) Integrated absorbance as a function of the angle of the transmission axis of an analyzing polarizer for the 2585.1 cm^{-1} line. Data have been fit with Eq. (2).

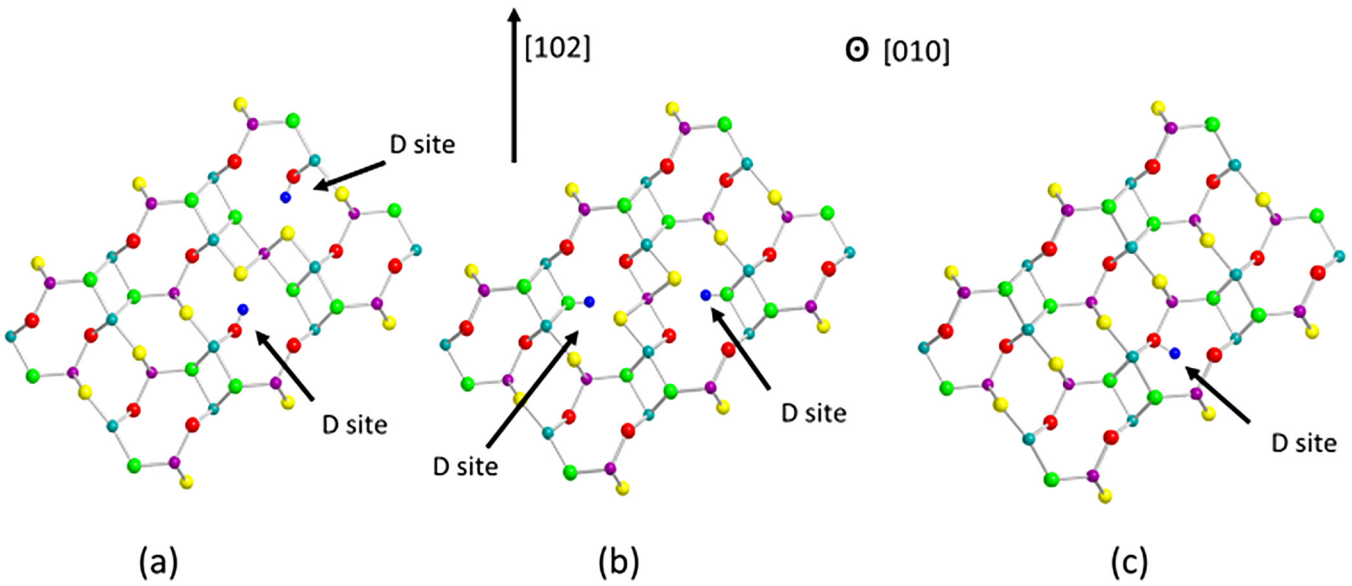

FIG. 11. (a) $V_{Ga(1)}$-2D complex with the "Kyrtsos" configuration of the shifted Ga(1) vacancy. (b) $V_{Ga(1)}$-2D complex with the "Varley" configuration of the shifted Ga(1) vacancy. (c) An interstitial D bonded to an O(1) atom. The inequivalent atomic sites are color coded as follows: Ga(1), purple; Ga(2), dark green; O(1), red; O(2), yellow; O(3), light green; and D, blue. These figures were constructed using MOLDRAW[56] and POV-Ray.[57]

In order to investigate the expected properties of perturbed OD defects in either Varley or interstitial configurations (as well as in other, less likely situations), theoretical calculations have been carried out on 80 or 120 atom supercells using the hybrid CRYSTAL17 code[47] with default relaxation criteria. Gaussian basis functions for most of the calculations were of the type 311p(1) for H (Ref. 48), 8411 for O (Ref. 49), 864111d41 for Ga (Ref. 50), 864111d41 for Fe (Ref. 51), 8511 for Mg (Ref. 52), 6621d for Si (Ref. 53), and 97631(511d) for Ge (Ref. 54).

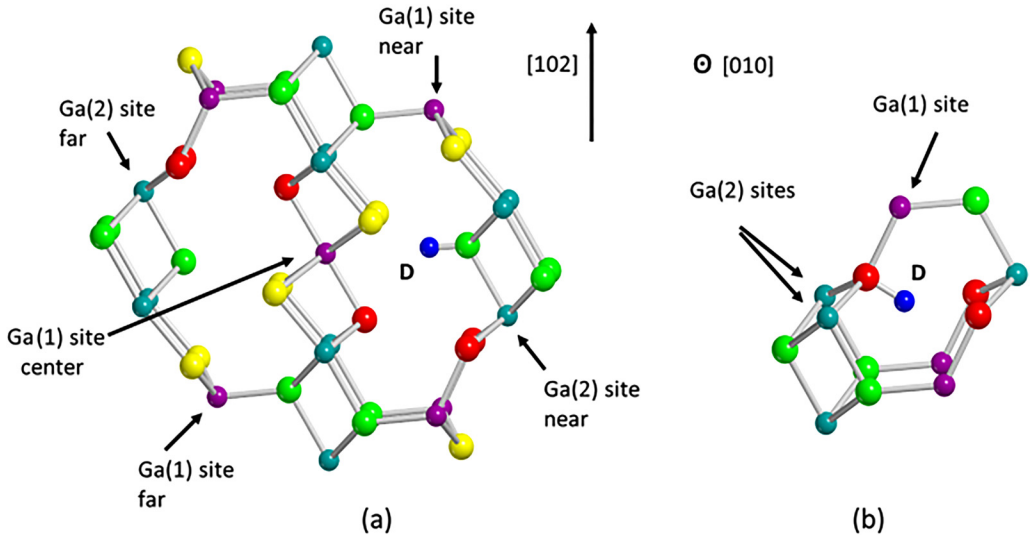

FIG. 12. Possible structures for the OD-impurity complexes. (a) shifted Ga(1) vacancy with a trapped D and candidate substitutional Ga sites for a metal impurity. (b) interstitial D trapped near candidate substitutional Ga sites for a metal impurity. The inequivalent atomic sites are color coded as follows: Ga(1), purple; Ga(2), dark green; O(1), red; O(2), yellow; O(3), light green; and D, blue. These figures were constructed using MOLDRAW[56] and POV-Ray.[57]

Figure 12 shows candidate configurations for the Varley case, with one trapped D, and likewise for the interstitial case. Ga(1) and Ga(2) sites that might contain a substitutional Mg or Fe [on Ga(2)] or Si or Ge [on Ga(1)] are shown. Other sites have also been investigated, but we focus on these at this time.

It has been shown recently by Mu *et al.*[55] (with which we agree) that H in a neutral Si–H complex (and presumably Ge–H) will not form an O–H bond but instead will bridge two Ga(1) sites, hydrogen-bond-like, in which case its vibrational frequencies will lie well below the O–H or O–D regions that we have investigated. This fact rules out the perturbed impurity-OH configuration [Fig. 12(b)] for Si and Ge.

Furthermore, our experimental results strongly suggest that all of the impurity-OH defects considered here are of the same "family": their frequencies are not widely separated and their transition moments are in the same orientation, well within experimental error. If this is the case, it eliminates a leading candidate that has been proposed for the Mg–H complex. Because of experimental evidence[28] suggesting that isolated Mg on a Ga(2) site can trap a hole on a neighboring O(1), it has seemed logical that isolated Mg, as well perhaps as Fe and other metal impurities, could also trap H^+ or D^+ on O(1) and indeed that model has been suggested by others[29] for the OD-Mg absorption that we have studied in this investigation.

Results of our calculations cast further doubt on the perturbed H interstitial model for these defect complexes. For all of the perturbed interstitial O–D cases that we have investigated, the O–D transition moment direction in the a–c plane will be within 2°–3° of 120° from [102]. This is well outside the range of the measured values. However, in all cases investigated, we find for the perturbed Varley case that the O–D direction is predicted to be within 2°–3° of 90° from [102]. This is on the edge of the range of experimental uncertainties for $\psi - |\chi|$ (Table II).

We find that, in general, the predicted O–D anharmonic frequencies are of order of 2500–2600 cm^{-1}, depending on the defect model and details of the calculation. While this spans the range seen experimentally, it is generally more fruitful to compare predicted vs experimental frequency *differences* for different impurities. In the trapped interstitial case, Fig. 12(b), with Mg or Fe on a Ga(2) site, it is difficult to rationalize the small frequency differences observed between the various impurities. Depending on the charge state or cluster size, these differences are predicted to be larger than 1–6 cm^{-1} as observed.

In the perturbed Varley case, Fig. 12(a), the predicted frequency differences are much smaller. For example, if the impurity Mg or Fe is trapped on the site labeled "Ga(2) site far," the anharmonic frequency for the OD-Fe center exceeds that for OD-Mg by ~2–5 cm^{-1}, a magnitude (but not sign) that is consistent with the experimental results presented here.

For the Si or Ge case, we find that for the perturbed Varley configurations, the predicted frequencies are less dependent on which nearby site, here a Ga(1) site, is considered for the Si or Ge. This may be because the nearest Ga(1) site is farther from the OD than was the case for the nearest Ga(2) site. So the Si could reside on near or far Ga(1) site and yield a predicted frequency several cm^{-1} lower than the Fe or Mg cases, consistent with the experiment. If the Si is on the Ga(1) "center" site in Fig. 12(a), the predicted frequency is higher than for Fe or Mg, so that site is probably not occupied by Si.

For Ge, for most of the Ga(1) sites, the predicted OD frequency is close to that for Si, whereas experimentally the OD frequency associated with Ge is 35 cm^{-1} lower than that for Si. We find such a large difference to exist if the impurity Ge is located on a Ga(2) site rather than Ga(1). Our calculations indicate that Ge is favored on a Ga(1) site by less than 0.2 eV, so it is not implausible that under the present experimental conditions the Ga(2) site is favored.

V. CONCLUSION

IR spectroscopy and theoretical analysis have been used to compare and contrast OD-impurity complexes in Ga_2O_3 for deep acceptors (Fe and Mg) and for shallow donors (Si and Ge). For the OD-Fe and OD-Mg complexes, we find O–D vibrational modes with very similar vibrational frequencies (within a few cm^{-1}) and very similar temperature dependences. Results in the literature for the OD-Zn complex suggest the similarity of this defect complex as well.[31] For the OD-Si and OD-Ge complexes, O–D modes in the same frequency range are observed but with a greater dependence on the identity of the trapped impurity. Furthermore, the polarization properties of all of the OD-impurity complexes we have studied yield transition-moment directions that are similar.

Theoretical analysis of likely configurations of the OD-impurity complexes suggests a family of defects based on a shifted Ga(1) vacancy (with the Varley configuration)[45] that traps H or D on an O(3) and with an additional impurity at a nearby Ga site [Fig. 12(a)]. If all of the OD-impurity complexes investigated here, for both the deep-acceptor and shallow-donor impurities, have this form, the similarity of their vibrational frequencies and transition moment directions is explained.

Having the deep acceptor impurity, Fe, Mg, or Zn, located at a "far" Ga(2) site [Fig. 12(a)], is consistent with the very similar vibrational frequencies and polarization properties of this group of OD-deep-acceptor complexes. Complexes based on a deep acceptor in the vicinity of an interstitial H or D[29,31] [Fig. 12(b)] are not consistent with the observed O–D directions or the small dependence of the O–D vibrational frequencies of the complexes on the identity of the deep acceptor. The apparent absence of the trapped H next to a deep acceptor is puzzling in view of the EPR evidence[28,32] for trapped holes at the deep acceptor and bears further consideration.

For the OD-shallow-donor complexes, the greater dependence of the vibrational frequency on the identity of the shallow donor leads us to suggest different configurations for these defects with possible candidates having the Si impurity trapped at one of the possible Ga(1) sites in Fig. 12(a) and having Ge trapped at a Ga(2) site. For the case of the OD-shallow-donor complexes, interstitial O–D configurations are ruled out by theory because of their high energy.[55] It is important to note, however, that the arguments for and against specific defect structures proposed here clearly cannot omit other (undiscovered) possibilities that may be suggested by further experimental and theoretical work.

ACKNOWLEDGMENTS

The Mg-doped sample studied here was grown at Synoptics. The work at Lehigh University was supported by NSF Grant No. DMR 1901563 (James Edgar) and an NSF REU site grant. E. R. Glaser acknowledges the support of the Office of Naval Research. The work at UF was performed as part of Interaction of Ionizing Radiation with Matter University Research Alliance (IIRM-URA), sponsored by the Department of the Defense, Defense Threat Reduction Agency under Award No. HDTRA1-20-2-0002 (Jacob Calkins). The content of the information does not necessarily reflect the position or the policy of the federal government, and no official endorsement should be inferred. The work at UF was also supported by NSF under No. DMR 1856662 (James Edgar). Portions of this research were conducted on Research Computing resources provided by Lehigh University supported by the NSF Award No. 2019035.

AUTHOR DECLARATIONS

Conflict of Interest

There is no conflict of interest to report.

DATA AVAILABILITY

The data that support the findings of this study are available from the corresponding author upon reasonable request.

REFERENCES

[1]M. Higashiwaki, A. Kuramata, H. Murakami, and Y. Kumagai, J. Phys. D: Appl. Phys. **50**, 333002 (2017).
[2]M. Higashiwaki and G. H. Jessen, Appl. Phys. Lett. **112**, 060401 (2018).
[3]J. Y. Tsao, S. Chowdhury, M. S. Hollis, D. Jena, N. M. Johnson, K. A. Jones, R. J. Kaplar, S. Rajan, C. G. Van de Walle, E. Bellotti, C. L. Chua, R. Collazo, M. E. Coltrin, J. A. Cooper, K. R. Evans, S. Graham, T. A. Grotjohn, E. R. Heller, M. Higashiwaki, M. S. Islam, P. W. Juodawlkis, M. A. Khan, A. D. Koehler, J. H. Leach, U. K. Mishra, R. J. Nemanich, R. C. N. Pilawa-Podgurski, J. B. Shealy, Z. Sitar, M. J. Tadjer, A. F. Witulski, M. Wraback, and J. A. Simmons, Adv. Electron. Mater. **4**, 1600501 (2018).
[4]S. J. Pearton, J. Yang, P. H. Cary, F. Ren, J. Kim, M. J. Tadjer, and M. A. Mastro, Appl. Phys. Rev. **5**, 011301 (2018).
[5]*Ga_2O_3: Technology, Devices and Applications*, edited by S. J. Pearton, F. Ren, and M. Mastro (Elsevier, Amsterdam, 2018).
[6]*Wide Bandgap Semiconductor-Based Electronics*, edited by F. Ren and S. J. Pearton (Institute of Physics Publishing, Bristol, 2020).
[7]J. Zhang, J. Shi, D.-C. Qi, L. Chen, and K. H. L. Zhang, "Recent progress on the electronic structure, defect, and doping properties of Ga_2O_3," APL Mater. **8**, 020906 (2020).
[8]S. Geller, J. Chem. Phys. **33**, 676 (1960).
[9]J. Åhman, G. Svensson, and J. Albertsson, Acta Cryst. **C52**, 1336 (1996).
[10]M. D. McCluskey, J. Appl. Phys. **127**, 101101 (2020).
[11]Z. Galazka, K. Irmscher, R. Uecker, R. Bertram, M. Pietsch, A. Kwasniewski, M. Naumann, T. Schulz, R. Schewski, D. Klimm, and M. Bickermann, J. Cryst. Growth **404**, 184 (2014).
[12]M. E. Ingebrigtsen, J. B. Varley, A. Y. Kuznetsov, B. G. Svensson, G. Alfieri, M. Mihaila, J. Badstübner, and L. Vines, Appl. Phys. Lett. **112**, 042104 (2018).
[13]P. D. C. King and T. D. Veal, J. Phys. Condens. Matter **23**, 334214 (2011).
[14]M. D. McCluskey, M. C. Tarun, and S. T. Teklemichael, J. Mater. Res. **27**, 2190 (2012).
[15]M. Stavola, W. B. Fowler, Y. Qin, P. Weiser, and S. J. Pearton, in *Ga_2O_3, Technology, Devices and Applications*, edited by S. J. Pearton, F. Ren, and M. Mastro (Elsevier, Amsterdam, 2018), Chap. 9, p. 191.
[16]J. B. Varley, J. R. Weber, A. Janotti, and C. G. Van de Walle, Appl. Phys. Lett. **97**, 142106 (2010).
[17]M. M. Islam, M. O. Liedke, D. Winarski, M. Butterling, A. Wagner, P. Hoseman, Y. Wang, B. Uberuaga, and F. A. Selim, Sci. Rep. **10**, 6134 (2020).
[18]P. Weiser, M. Stavola, W. B. Fowler, and Y. Qin, Appl. Phys. Lett. **112**, 232104 (2018).
[19]M. Stavola, in *Identification of Defects in Semiconductors*, edited by M. Stavola (Academic, Boston, MA, 1998), Chap. 3, Vol. 51B, p. 153.
[20]M. Stavola and W. B. Fowler, J. Appl. Phys. **123**, 161561 (2018).
[21]A. Portoff, A. Venzie, M. Stavola, W. B. Fowler, and S. Pearton, J. Appl. Phys. **127**, 055702 (2020).
[22]E. G. Villora, K. Shimamura, Y. Koshikawa, T. Ujiie, and K. Aoki, Appl. Phys. Lett. **92**, 202120 (2008).
[23]S.-H. Han, A. Mauze, E. Ahmadi, T. Mates, Y. Oshima, and J. S. Speck, Semicond. Sci. Technol. **33**, 045001 (2018).
[24]K. Irmscher, Z. Galazka, M. Pietsch, R. Uecker, and R. Fornari, J. Appl. Phys. **110**, 063720 (2011).
[25]N. T. Son, K. Goto, K. Nomura, Q. T. Thieu, R. Togashi, H. Murakami, Y. Kumagai, A. Kuramata, M. Higashiwaki, A. Koukitu, S. Yamakoshi, B. Monemar, and E. Janzén, J. Appl. Phys. **120**, 235703 (2016).
[26]C. A. Lenyk, T. D. Gustafson, L. E. Halliburton, and N. C. Giles, J. Appl. Phys. **126**, 245701 (2019).
[27]S. Bhandari, M. E. Zvanut, and J. B. Varley, J. Appl. Phys. **126**, 165703 (2019).
[28]B. E. Kananen, L. E. Halliburton, E. M. Scherrer, K. T. Stevens, G. K. Foundos, K. B. Chang, and N. C. Giles, Appl. Phys. Lett. **111**, 072102 (2017).
[29]J. R. Ritter, J. Huso, P. T. Dickens, J. B. Varley, K. G. Lynn, and M. D. McCluskey, Appl. Phys. Lett. **113**, 052101 (2018).
[30]H. Peelaers, J. L. Lyons, J. B. Varley, and C. G. Van de Walle, APL Mater. **7**, 022519 (2019).
[31]C. Pansegrau, J. Jesenovec, J. S. McCloy, and M. D. McCluskey, Appl. Phys. Lett. **119**, 102104 (2021).
[32]T. D. Gustafson, J. Jesenovec, C. A. Lenyk, N. C. Giles, J. S. McCloy, M. D. McCluskey, and L. E. Halliburton, J. Appl. Phys. **129**, 155701 (2021).
[33]A. Y. Polyakov, N. B. Smirnov, I. V. Shchemerov, S. J. Pearton, F. Ren, A. V. Chernykh, and A. I. Kochkova, Appl. Phys. Lett. **113**, 142102 (2018).
[34]A. Venzie, A. Portoff, C. Fares, M. Stavola, W. B. Fowler, F. Ren, and S. J. Pearton, Appl. Phys. Lett. **119**, 062109 (2021).
[35]J. R. Ritter, K. G. Lynn, and M. D. McCluskey, Proc. SPIE **10919**, 109190Z (2019).
[36]J. R. Ritter, K. G. Lynn, and M. D. McCluskey, J. Appl. Phys. **126**, 225705 (2019).
[37]R. Sharma, M. E. Law, M. Xian, M. Tadjer, E. A. Anber, D. Foley, A. C. Lang, J. L. Hart, J. L. Hart, J. Nathaniel, M. L. Taheri, F. Ren, S. J. Pearton, and A. Kuramata, J. Vac. Sci. Technol. B **37**, 051204 (2019).
[38]C. Sturm, J. Furthmüller, F. Bechstedt, R. Schmidt-Grund, and M. Grundmann, APL Mater. **3**, 106106 (2015).
[39]EAG Laboratories, private communication (11 August 2021).
[40]A. Kuramata, K. Koshi, S. Watanabe, Y. Yamaoka, T. Masui, and S. Yamakoshi, in *Proceedings of SPIE, Oxide-Based Materials and Devices IX* (SPIE, 2018), Vol. 10533, p. 105330E.
[41]Y. Qin, M. Stavola, W. B. Fowler, P. Weiser, and S. J. Pearton, ECS J. Solid State Sci. Technol. **8**, Q3103 (2019).
[42]B. N. J. Persson and R. Ryberg, Phys. Rev. B **32**, 3586 (1985).
[43]G. Turrell, *Infrared and Raman Spectra of Crystals* (Academic Press, London, 1972).
[44]A. Portoff, A. Venzie, Y. Qin, M. Stavola, W. B. Fowler, and S. J. Pearton, ECS J. Solid State Sci. Technol. **9**, 125006 (2020).
[45]J. B. Varley, H. Peelaers, A. Janotti, and C. G. Van de Walle, J. Phys. Condens. Matter **23**, 334212 (2011).
[46]A. Krytsos, M. Matsubara, and E. Bellotti, Phys. Rev. B **95**, 245202 (2017).

[47]R. Dovesi, A. Erba, R. Orlando, C. M. Zicovich-Wilson, B. Civalleri, L. Maschio, M. Ŕerat, S. Casassa, J. Baima, S. Salustro, and B. Kirtman, "Quantum-mechanical condensed matter simulations with crystal," WIREs Comput. Mol. Sci. **8**, e1360 (2018).
[48]R. Krishnan, J. S. Binkley, R. Seeger, and J. A. Pople, J. Chem. Phys. **72**, 650 (1980).
[49]J. E. Jaffe and A. C. Hess, Phys. Rev. B **48**, 7903 (1993).
[50]R. Pandey, J. E. Jaffe, and N. M. Harrison, J. Phys. Chem. Solids **55**, 1357 (1994).
[51]M. Catti, G. Valerio, and R. Dovesi, Phys. Rev. B **51**, 7441 (1995).
[52]M. I. McCarthy and N. M. Harrison, Phys. Rev. B **49**, 8574 (1994).
[53]R. Nada, C. R. A. Catlow, R. Dovesi, and C. Pisani, Phys. Chem. Miner. **17**, 353 (1990).
[54]G. Sophia, P. Baranek, C. Sarrazin, M. Rerat, and R. Dovesi, from the basis set compilation in www.crystal.unito/it.
[55]S. Mu, M. Wang, J. B. Varley, J. L. Lyons, D. Wickramaratne, and C. G. Van de Walle, arXiv:2111.07194v1 [cond-mat.mtrl-sci] (13 November 2021).
[56]P. Ugliengo, see http://moldraw.unito.it for "MOLDRAW" (2006).
[57]See http://povray.org for "POV-Ray."